Coupling of gap plasmons in multi-wire waveguides

A. Manjavacas and F. J. García de Abajo*

Instituto de Óptica - CSIC and Unidad Asociada CSIC-Universidade de Vigo, Serrano 121, 28006 Madrid, Spain

* jga@cfmac.csic.es

Abstract: We investigate the coupling of gap plasmons in various configurations of neighboring metallic nanowires. Starting with the basic element defining a gap plasmon, consisting of two neighboring silver wires, we study the energy splitting and symmetry properties of hybridized plasmons resulting from the interaction of two wire pairs. The system is shown to display non-avoided crossings of hybridized modes, and it evolves at short distances towards a degenerate system consisting of four wires arranged in a square, where two new gap plasmons emerge from redshifted higher-energy modes. The gap modes of three neighboring wires are also described in a continuous transition from a coplanar configuration to an equilateral triangle arrangement. The interaction between wire pairs is shown to be weak enough to prevent efficient transfer of plasmon signal from a pair to the other one, which is beneficial to avoid crosstalking, but not to produce waveguide couplers. The coupling is significantly increased by placing a wire of rectangular cross section in between the wire pairs, thus allowing us to achieve large plasmon-signal transfers within propagation distances below the attenuation length. Our results can find application in the design of signal-processing devices based upon gap plasmons.

OCIS codes: (250.5403) Plasmonics; (240.6680) Surface plasmons; (230.7370) Waveguides.

References and links

1. P. Berini, "Plasmon-polariton waves guided by thin lossy metal films of finite width: Bound modes of symmetric structures," Phys. Rev. B **61**, 10484–10503 (2000).
2. P. Berini, "Plasmon-polariton waves guided by thin lossy metal films of finite width: Bound modes of asymmetric structures," Phys. Rev. B **63**, 125417 (2001).
3. J. D. Jackson, *Classical Electrodynamics* (Wiley, New York, 1999).
4. J. R. Krenn, A. Dereux, J. C. Weeber, E. Bourillot, Y. Lacroute, J. P. Goudonnet, G. Schider, W. Gotschy, A. Leitner, F. R. Aussenegg, and C. Girard, "Squeezing the optical near-field zone by plasmon coupling of metallic nanoparticles," Phys. Rev. Lett. **82**, 2590–2593 (1999).
5. S. A. Maier, P. G. Kik, H. A. Atwater, S. Meltzer, E. Harel, B. E. Koel, and A. A. G. Requicha, "Local detection of electromagnetic energy transport below the diffraction limit in metal nanoparticle plasmon waveguides," Nat. Mater. **2**, 229–232 (2003).
6. S. I. Bozhevolnyi, V. S. Volkov, E. Devaux, J. Y. Laluet, and T. W. Ebbesen, "Channel plasmon subwavelength waveguide components including interferometers and ring resonators," Nature **440**, 508–511 (2006).
7. E. Moreno, S. G. Rodrigo, S. I. Bozhevolnyi, L. Martín-Moreno, and F. J. García-Vidal, "Guiding and focusing of electromagnetic fields with wedge plasmon polaritons," Phys. Rev. Lett. **100**, 023901 (2008).
8. G. Veronis and S. Fan, "Guided subwavelength plasmonic mode supported by a slot in a thin metal film," Opt. Lett. **30**, 3359–3361 (2005).
9. A. Manjavacas and F. J. García de Abajo, "Robust plasmon waveguides in strongly interacting nanowire arrays," Nano Lett. **9**, 1285–1289 (2009).

#116060 - $15.00 USD Received 24 Aug 2009; revised 23 Sep 2009; accepted 24 Sep 2009; published 12 Oct 2009

10. R. F. Oulton, V. J. Sorger, D. A. Genov, D. F. P. Pile, and X. Zhang, "A hybrid plasmonic waveguide for subwavelength confinement and long-range propagation," Nat. Phot. **2**, 496–500 (2008).
11. J. A. Conway, S. Sahni, and T. Szkopek, "Plasmonic interconnects versus conventional interconnects: A comparison of latency, crosstalk and energy costs," Opt. Express **15**, 4474–4484 (2007).
12. G. Veronis and S. Fan, "Crosstalk between three-dimensional plasmonic slot waveguides," Opt. Express **16**, 2129–2140 (2008).
13. F. J. García de Abajo, A. Rivacoba, N. Zabala, and P. M. Echenique, "Electron energy loss spectroscopy as a probe of two-dimensional photonic crystals," Phys. Rev. B **68**, 205105 (2003).
14. F. J. García de Abajo and A. Howie, "Retarded field calculation of electron energy loss in inhomogeneous dielectrics," Phys. Rev. B **65**, 115418 (2002).
15. F. J. García de Abajo and M. Kociak, "Probing the photonic local density of states with electron energy loss spectroscopy," Phys. Rev. Lett. **100**, 106804 (2008).
16. P. B. Johnson and R. W. Christy, "Optical constants of the noble metals," Phys. Rev. B **6**, 4370–4379 (1972).
17. E. D. Palik, *Handbook of Optical Constants of Solids* (Academic Press, New York, 1985).
18. L. D. Landau and E. M. Lifshitz, *Quantum Mechanics: Non-Relativistic Theory* (Pergamon Press, Oxford, 1981).
19. I. N. Levine, *Molecular Spectroscopy* (Wiley-Interscience, London, 1975).
20. P. R. McIsaac, "Symmetry-induced modal characteristics of uniform waveguides - I: Summary of results," IEEE Trans. Microwave Theory Tech. **23**, 421–429 (1975).
21. P. R. McIsaac, "Symmetry-induced modal characteristics of uniform waveguides - II: Theory," IEEE Trans. Microwave Theory Tech. **23**, 429–433 (1975).

1. Introduction

Collective excitations of conduction electrons near metal surfaces can mix with electromagnetic fields to produce surface plasmon polaritons, which are capable of propagating over hundreds of microns along metal surfaces [1, 2]. These excitations are however confined to the surface and penetrate inside the metal only a few tens of nanometers (the skin depth [3]). In planar metal-dielectric interfaces, plasmons extend towards the dielectric over a significant fraction of a micron at visible and near-infrared frequencies, but this spreading can be limited by conveniently shaping the interface, so that the overall extension of the mode in the plane perpendicular to the propagation direction is reduced to just a few nanometers in average radius. These properties make surface plasmons very attractive as carriers of information that can be highly packed in space. Several designs have been proposed to this end, including particle chains [4, 5] and plasmons propagating along grooves [6], wedges [7], gaps between metals [8, 9], and metallodielectric structures [10]. Among these, the modes defined in the gap between two metal wires have been shown to be particularly robust against sharp turnings and wire imperfections, and they allow optimum three-dimensional integration with minimum crosstalk [9]. Actually, crosstalking is a limiting factor in the achievable degree of integration, with dramatic effects in single wires [11], but it is largely reduced in gap plasmons [12].

In this paper, we explore the hybridization of gap plasmons in aligned metal wires. In particular, we study the interaction between the gap modes of two neighboring wire-pairs as a function of the spacing between them. The interaction of gap modes in a system formed by three wires is also investigated. We conclude with a proposal of a gap-mode coupler consisting of an intermediate rectangular wire that can produce large transfer of the gap mode from a given wire pair to a neighboring one. We obtain the dispersion relation of gap modes by examining the photonic density of states (DOS), which is derived from the solution of Maxwell's equations for an arbitrary number of circular wires using two-dimensional multiple elastic scattering of multipole expansions (2D-MESME) of the field around the cylinders [13]. We also look into the photonic local density of states (LDOS) using a boundary element method (BEM) for translationally invariant (but otherwise arbitrary) geometries [14] (see Appendix). The LDOS is defined by analogy to its electronic counterpart as the combined local intensity of all eigenmodes of the system under investigation, and it takes the value $\omega^2\varepsilon^{1/2}/3\pi^2c^3$ in a homogeneous medium of permittivity ε when projected along any spatial direction. In fact, we decompose this quantity into the contribution of different wavevectors q along the direction of translational symmetry

#116060 - $15.00 USD Received 24 Aug 2009; revised 23 Sep 2009; accepted 24 Sep 2009; published 12 Oct 2009

z. For example, in a homogeneous medium, the q-resolved LDOS projected along z reduces to $(\omega/2\pi c^2)(1-q^2/q_\varepsilon^2)\theta(q_\varepsilon - q)$, where $q_\varepsilon = \omega\varepsilon^{1/2}/c$ [15]. The q-resolved DOS is the integral of the LDOS over the remaining $x-y$ directions. Our BEM requires 200 points per wire in order to achieve convergence within the scale of the plots; the computation time scales with the cube of the number of cylinders and it takes less than a minute for each value of (q,ω) in a wire-pair system using an ordinary workstation. Regarding the 2D-MESME method, we have achieved convergence by including multipoles with azimuthal quantum numbers up to $m = 20$, and each value of (q,ω) takes less than a second for a system formed by two wires.

2. Interaction between gap plasmons

The basic element defining a gap plasmon is the wire pair depicted in Fig. 1(a). In what follows, we focus on silver wires of circular cross section and 200 nm in diameter embedded in a silica matrix. The silver [16] and silica [17] are described by their measured complex dielectric functions. The plasmon modes of this system are unveiled in the dispersion diagram of Fig. 1(c), which shows the photonic DOS as a function of photon energy $\hbar\omega$ and momentum $\hbar q$ along the wires, encompassing a dependence on time t and propagation distance z given by $\exp[\mathrm{i}(qz-\omega t)]$. The guided modes of the wire pair lie outside the light cone of the embedding silica, and one of them is clearly isolated from the rest, with significantly larger values of q that make it more confined [9]. This so-called gap plasmon is bound to the gap region between the wires, as shown in the inset of Fig. 1(c).

The interaction between wire pairs placed at a distance b [see Fig. 1(b)] is investigated in Fig. 2. At large distances, the interaction between gap modes is weak and results in a small energy splitting that increases as b becomes smaller [see Fig. 2(a)]. This is accompanied by a significant redshift in two of the higher-energy modes. Eventually the splitting of the two gap modes decreases with decreasing b, presumably as a result of mode repulsion triggered by the approaching higher-energy modes, at there is even a non-avoided mode crossing, which is clearly resolved in the zoomed inset of Fig. 2(a).

It is surprising to see that the gap modes undergo such a non-avoided crossing, since it is clear that they interact with each other even at relatively large distances within the range considered in Fig. 2. That is, their interaction is allowed by symmetry, but they still cross each other. The reason for this is that the interaction becomes zero exactly at the point of crossing, thus averting the typical avoided-crossing behavior described in quantum chemistry textbooks [18]. This is actually a feature associated to the interaction between line dipoles in two dimensions. Unlike the interaction between point dipoles, which is described in free space by the non-vanishing complex dipole field, line dipoles can have vanishing interaction. This is illustrated by the electric field created under the conditions of Fig. 3, where we represent the field due to a line dipole of the form $\mathrm{e}^{\mathrm{i}qz}\hat{\mathbf{y}}$, placed in a homogeneous medium of permittivity ε and with the line oriented along z. The electric field at points along the x axis takes the form

$$\mathbf{E}(R\hat{\mathbf{x}}) = 2\left[k^2 K_0(\Gamma R) - \frac{\Gamma}{\varepsilon R}K_1(\Gamma R)\right]\mathrm{e}^{\mathrm{i}qz}\,\hat{\mathbf{y}}, \tag{1}$$

where $k = 2\pi/\lambda$ is the light wavevector in free space, $\Gamma = \sqrt{q^2-\varepsilon k^2}$, and K_0 and K_1 are modified Bessel functions. The interaction is thus real (for $q > \varepsilon^{1/2}k$ outside the light cone of the medium), except for a trivial plane wave dependence on z, and it contains a node at a distance $R = 306\,\mathrm{nm}$ from the z axis for $\lambda = 1605\,\mathrm{nm}$. The center-to-center distance at the crossing point in the wires of Fig. 2 is 213 nm. This is qualitatively consistent with the line-dipole model (Fig. 3), which is an idealization of the field produced by a gap mode.

The orientation of the electric field in the gap regions of two interacting wire-pairs is schematically represented in Fig. 2(b). A detailed account of the derivation of these schemes

#116060 - $15.00 USD Received 24 Aug 2009; revised 23 Sep 2009; accepted 24 Sep 2009; published 12 Oct 2009

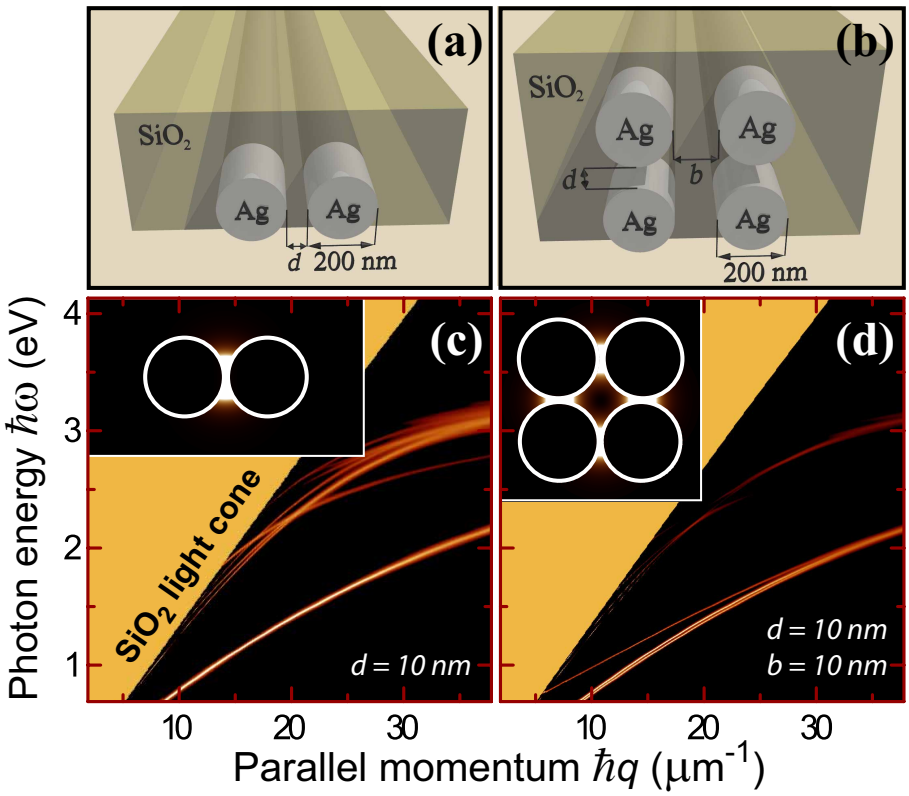

Fig. 1. Gap plasmon modes for one and two wire-pairs. (a)-(b) Schematic view of the geometry. (c)-(d) Photonic density of states (DOS) as a function of energy and momentum parallel to the wires for one and two wire-pairs. The inter-wire gap distance is $d = 10$ nm in both cases and the distance b between the two wire-pairs in (d) is 10 nm. The insets show the spatial distribution of the local density of states (LDOS) for the lowest-energy gap mode at a free-space light wavelength of 1550 nm. Brighter regions correspond to higher DOS and LDOS values.

is given in the Appendix. At large distances, a characteristic binding-antibinding interplay is displayed (panels 4 and 5). Incidentally, parallel dipoles (panel 5) give rise to binding (lower energy), although this behavior is reversed at small distances due to the sign change noted in Eq. (1) and Fig. 3.

An interesting situation is presented when the distance between all wires is the same [$b = d = 10$ nm in Fig. 1(d) and Fig. 2], so that there are four hybridized gap modes. In the evolution of different modes when two wire-pairs are brought together into this configuration [Fig. 2(a)], we find that one of the higher-order modes is dramatically redshifted to become degenerate with a short-distance antibinding mode [panel 2 of Fig. 2(b)].The binding mode [panel 1] involves electric fields of adjacent gaps facing each other. The remaining fourth mode is provided by another redshifted higher-order mode, and displays closed electric-field lines, which make it more strongly confined. For completeness, the dispersion diagram of this degenerate system is given in Fig. 1(d), showing three gap-mode lines that are clearly separated from the upper-energy structure: a central line corresponding to the two degenerate modes of panel 2 in Fig. 2(b), flanked by two non-degenerate lines [upper and lower lines in Fig. 1(d),

#116060 - $15.00 USD Received 24 Aug 2009; revised 23 Sep 2009; accepted 24 Sep 2009; published 12 Oct 2009

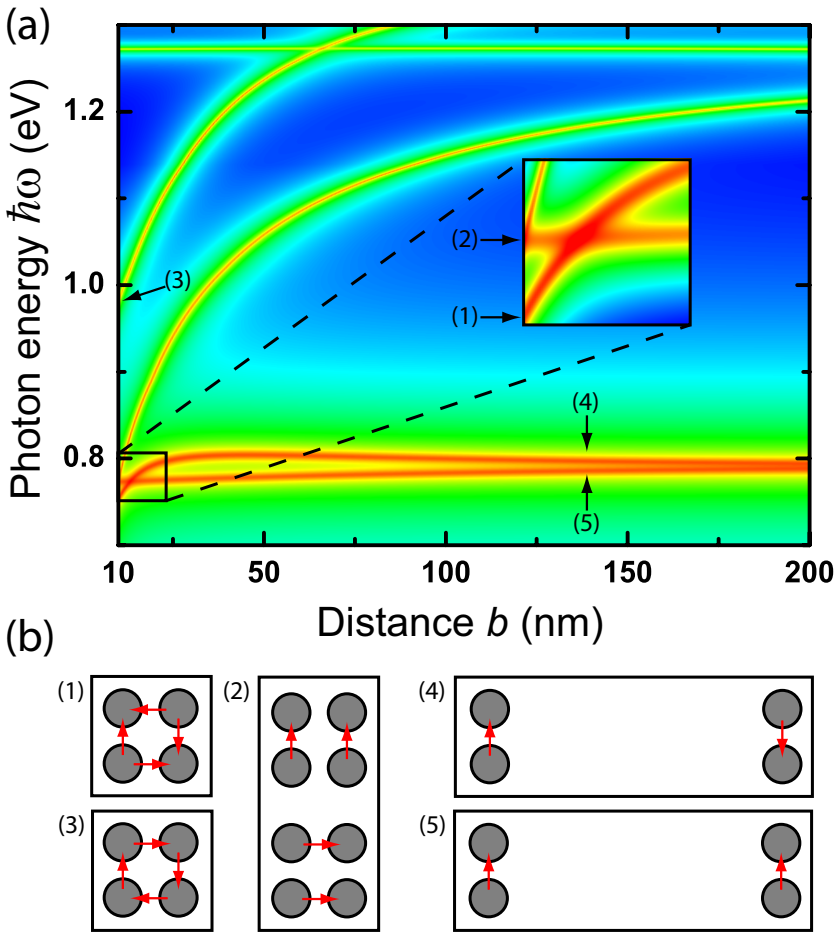

Fig. 2. (a) Evolution of the modes in two wire-pairs as a function of the distance between them for fixed $q = 10\,\mu\mathrm{m}^{-1}$. The inset shows a zoom of the low-energy mode-crossing region. (b) Orientation of the electric field in the gap regions for two limiting geometries: (1-3) square symmetry ($b = d = 10\,\mathrm{nm}$) and (4,5) rectangular symmetry ($b \gg d = 10\,\mathrm{nm}$). The numerical labels correspond to the modes signalled by arrows in (a). The symmetry increase in the square configuration leads to mode degeneracy, as shown in (3).

#116060 - $15.00 USD Received 24 Aug 2009; revised 23 Sep 2009; accepted 24 Sep 2009; published 12 Oct 2009

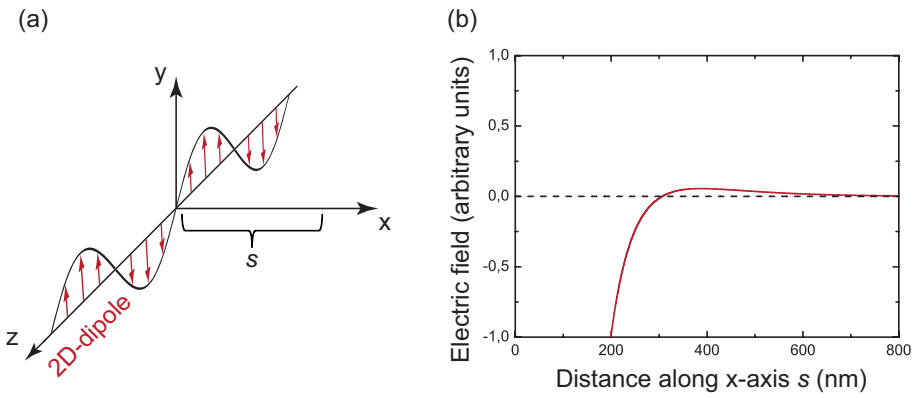

Fig. 3. Spatial dependence of field produced by a line dipole. (a) Line of dipoles $e^{iqz}\hat{\mathbf{y}}$ distributed along the z axis. (b) y component of the electric field produced by the dipoles of (a) along the x axis for a free-space wavelength $\lambda = 1605\,\text{nm}$ and $q = 10\,\mu\text{m}^{-1}$, with the dipoles embedded in silica ($\varepsilon = 2.08$).

corresponding to the modes of panels 3 and 1 in Fig. 2(b), respectively]. This mode structure can be qualitatively described by considering the interaction of nearest-neighbors gap-plasmons described by a coupling energy Δ and leading to the interaction matrix

$$\begin{bmatrix} 0 & \Delta & 0 & \Delta \\ \Delta & 0 & \Delta & 0 \\ 0 & \Delta & 0 & \Delta \\ \Delta & 0 & \Delta & 0 \end{bmatrix},$$

which has two degenerate eigenstates $(0,-1,0,1)$ and $(-1,0,1,0)$ at the same energy as the single wire-pair [these are the modes of panel 2 in Fig. 2(b)], a state $(-1,1,-1,1)$ shifted by -2Δ (panel 3), and another state $(1,1,1,1)$ shifted by 2Δ (panel 1, implying that $\Delta < 0$). Notice that the two degenerate eigenstates $(0,-1,0,1)$ and $(-1,0,1,0)$ form a basis of the 2-dimensional irreducible representation E of the point group C_{4v}, which characterizes the coupled square structure. In the same way, the other two eigenstates $(-1,1,-1,1)$ and $(1,1,1,1)$ form a basis of the 1-dimensional irreducible representations B_2 and A_2, respectively [19]. This means that each of those eigenstates is transformed under the symmetry operations, as each irreducible representation indicates. It should be mentioned that a systematic analysis of the modes of systems with square symmetry leads to six types of modes (two degenerate ones and four non-degenerate) [20, 21], but here we are concerned only with modes that are a combination of gap modes, and therefore, this restriction limits our number of states to just four. The coordinates in the vectors stand for the electric field in consecutive gaps of the structure (e.g., -1 and 1 correspond to clockwise and counterclockwise orientations of the field, respectively). Whereas this model predicts a symmetric disposition of the upper- and lower-energy gap states relative to the unperturbed state, the $(-1,1,-1,1)$ state undergoes much larger shift than the $(1,1,1,1)$ state in the actual structure [Fig. 2(a)], which we attribute to interaction with higher other states, although the effect of second-neighbor interaction cannot be ruled out. Incidentally, this type of interaction does not change the symmetry of the states.

The hybridization of gap modes in a wire trimer is studied in Fig. 4. Starting from a coplanar configuration (i.e., a trimer angle of 180°), the interaction increases as the angle spanned by the two gaps is reduced, thus leading to further splitting between the energies of the two resulting

#116060 - $15.00 USD Received 24 Aug 2009; revised 23 Sep 2009; accepted 24 Sep 2009; published 12 Oct 2009

hybridized modes. Interestingly, the splitting reaches a maximum at an angle of $\sim 70^\circ$, and it drops to zero in the 3-fold symmetric trimer (angle $= 60^\circ$). A higher-order mode is redshifted with decreasing trimer angle, and becomes the third mode of the symmetric trimer. The degeneracy of two of the three gap modes is needed by symmetry in this case, as deduced from the interaction matrix

$$\begin{bmatrix} 0 & \Delta' & \Delta' \\ \Delta' & 0 & \Delta' \\ \Delta' & \Delta' & 0 \end{bmatrix},$$

where Δ' represents the inter-mode coupling. This matrix has two degenerate eigenmodes, $(1,0,-1)$ and $(-1,1,0)$, with energy shift $-\Delta'$ and a symmetric mode, $(1,1,1)$, shifted by $2\Delta'$. These states form a basis of the irreducible representations E (2-dimensional) and A_2 (1-dimensional) of the point group C_{3v}, which characterizes the 3-fold-symmetric trimer-structure. They are in full agreement with the orientation of the electric field at the gaps of the symmetric trimer (see left insets in Fig. 4 and also the Appendix), although the relative energy shift is larger for the symmetric mode in the actual structure, presumably as a result of interaction with higher-energy modes. Again, the restriction that the hybridized modes are made of gap modes limits their number to just three, rather than the four states predicted by general symmetry theory for structures with triangular symmetry [20, 21].

3. A gap plasmon coupler

The coupling between gap modes in the two wire-pairs of Fig. 1(b) is relatively weak according to Fig. 2(a), except at very small distances b. The crosstalk between gap plasmons is then small, also implying that it will be difficult to realize a plasmon coupler capable of transferring a plasmon signal from a given wire-pair to a neighboring one (see below). We intend however to design a plasmon coupler for wire pairs, that is an important element in eventual plasmonic circuits for implementing simple logical elements such as splitters and interferometers [6].

We need to estimate how much of the signal propagating in a gap-plasmon mode is transferred to another neighboring gap plasmon over a certain propagation distance. Following Ref. [12], we note that for symmetric systems such as those considered above there exist (for any given fixed frequency) two hybridized gap modes that are symmetric and antisymmetric with respect to the center of the combined structure. We can write them as

$$\begin{aligned} \mathbf{E}_s(\mathbf{r}) &= \mathbf{e}_s(x,y)\,\mathrm{e}^{\mathrm{i}q_s z}, \\ \mathbf{E}_a(\mathbf{r}) &= \mathbf{e}_a(x,y)\,\mathrm{e}^{\mathrm{i}q_a z}, \end{aligned}$$

where q_s and q_a are the corresponding wavevectors along the direction of the wires. These two modes can be expressed as symmetric and antisymmetric combinations of the gap modes of each wire pair (1 and 2) as

$$\begin{aligned} \mathbf{e}_s &= \frac{1}{\sqrt{2}}\left[\mathbf{e}_1 + \mathbf{e}_2\right], \\ \mathbf{e}_a &= \frac{1}{\sqrt{2}}\left[\mathbf{e}_1 - \mathbf{e}_2\right]. \end{aligned}$$

Now, we can prepare a signal that is propagating in a combined state

$$\begin{aligned} \mathbf{E}(\mathbf{r}) &= \frac{1}{\sqrt{2}}\left[\mathrm{e}^{\mathrm{i}q_s z}\mathbf{e}_s(x,y) + \mathrm{e}^{\mathrm{i}q_a z}\mathbf{e}_a(x,y)\right] \\ &= \frac{1}{2}\left(\mathrm{e}^{\mathrm{i}q_s z} + \mathrm{e}^{\mathrm{i}q_a z}\right)\mathbf{e}_1(x,y) + \frac{1}{2}\left(\mathrm{e}^{\mathrm{i}q_s z} - \mathrm{e}^{\mathrm{i}q_a z}\right)\mathbf{e}_2(x,y). \end{aligned}$$

#116060 - $15.00 USD Received 24 Aug 2009; revised 23 Sep 2009; accepted 24 Sep 2009; published 12 Oct 2009

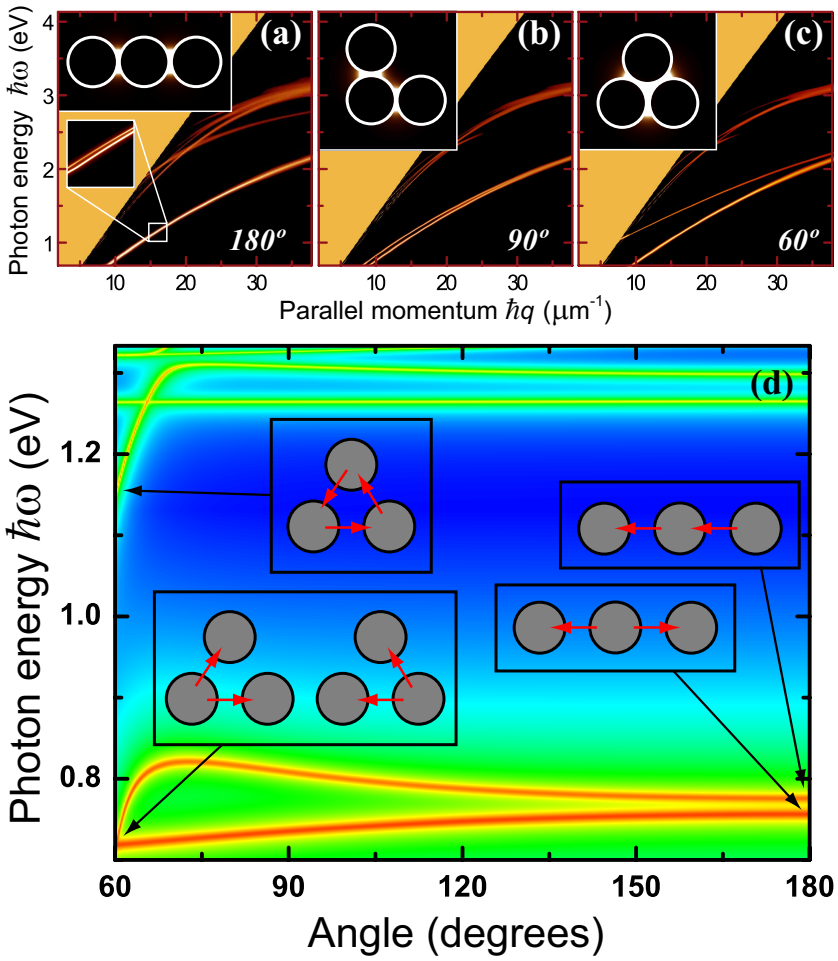

Fig. 4. Gap modes in a wire trimer. (a)-(c) Photonic density of states (DOS) as a function of energy and momentum parallel to the wires for three different trimer-angles. The insets show the spatial distribution of the local density of states (LDOS) for the lowest-energy gap mode at a free-space light wavelength of 1550 nm. (d) Evolution of the gap modes with the trimer angle for fixed $q = 10\,\mu\mathrm{m}^{-1}$. The insets show the orientation of the electric field in the gap regions for equilateral and coplanar trimers. Two of the modes are degenerate in the 3-fold symmetric case (angle $= 60^{\circ}$). The inter-wire gap distance is $d = 10\,\mathrm{nm}$ in all cases.

#116060 - $15.00 USD Received 24 Aug 2009; revised 23 Sep 2009; accepted 24 Sep 2009; published 12 Oct 2009

This state is initially propagating in the gap mode 1 at $z = 0$ (the coefficient of state $\mathbf{e}_2$ vanishes at that point). The fraction of power $T(L)$ that is transferred to mode 2 after propagation over a distance L is given by the squared modulus of the coefficient multiplying $\mathbf{e}_2$ [12]:

$$T(L) = \frac{1}{4}\left|e^{iq_sL} - e^{iq_aL}\right|^2. \tag{2}$$

If we neglect absorption, q_s and q_a are real, so that Eq. (2) reduces to

$$T(L) = \sin^2\left[(q_s - q_a)L/2\right],$$

which is an oscillatory function of L predicting full transfer from gap 1 to gap 2 after a propagation distance $L = \pi/|q_s - q_a|$. However, absorption introduces a small imaginary part in the wavevectors, leading to attenuated oscillations.

We represent in Fig. 5(b) a representative case of the fraction of transferred power $T(L)$ between two wire-pairs (dashed curve), given by Eq. (2) for the values of q_s and q_a obtained from BEM with $b = 20\,\text{nm}$ and $\lambda = 1550\,\text{nm}$. The maximum transferred-power fraction is only $T_{\max} = 35.6\%$. The remaining power is lost to absorption before full transfer between gap modes can be realized. This coupling scheme is thus of no practical use because absorption dominates over power transfer. In order to increase the coupling efficiency, we have placed a structure in between the wire pairs [see Fig. 5(a)], leading to a larger maximum transferred-power fraction $T_{\max} = 74.3\%$, as shown by the solid curve of Fig. 5(b). This geometry is not fully optimized, but it shows that by placing a structure in between the waveguides, one can increase crosstalking to achieve a significant degree of power transfer. This type of coupler can find practical application in waveguide splitters, interferometers, and other signal processing elements.

4. Conclusion

In summary, we have shown that the interaction of gap plasmons confined to wire-pairs leads to a complex structure of hybridized modes, including non-avoided crossings facilitated by the vanishing of the interaction right at the point of crossing. We find that the coupling between wire pairs is not strong enough to allow complete transfer of plasmon signal between pairs within a propagation distance well below the attenuation length (it reaches a transfer fraction of 35% for short distances, but it is generally lower; this is a consequence of the robustness of these gap plasmons against undesired crosstalking [9]). As an alternative, we have presented a design of a more efficient plasmon coupler containing an additional intermediate wire and capable of transferring 74% of the signal between wires. This illustrates the advantage of adding such an additional wire, although we have not tried to optimized the geometry to achieve the maximum possible transfer rate. Optimization of geometrical parameters should allow achieving larger transfer fractions for application to signal-processing elements such as waveguide splitters, energy filters, and interferometers.

Appendix: Calculation of LDOS and plasmon-mode spatial profiles

The photonic eigenmodes of a system fully characterize its optical response. Their *wave functions* correspond to the electric fields $\mathbf{E}_j$, which satisfies Maxwell's equations,

$$\nabla \times \nabla \times \mathbf{E}_j(\mathbf{r}) - \frac{\omega_j^2}{c^2}\varepsilon(\mathbf{r})\mathbf{E}_j(\mathbf{r}) = 0. \tag{3}$$

#116060 - $15.00 USD Received 24 Aug 2009; revised 23 Sep 2009; accepted 24 Sep 2009; published 12 Oct 2009

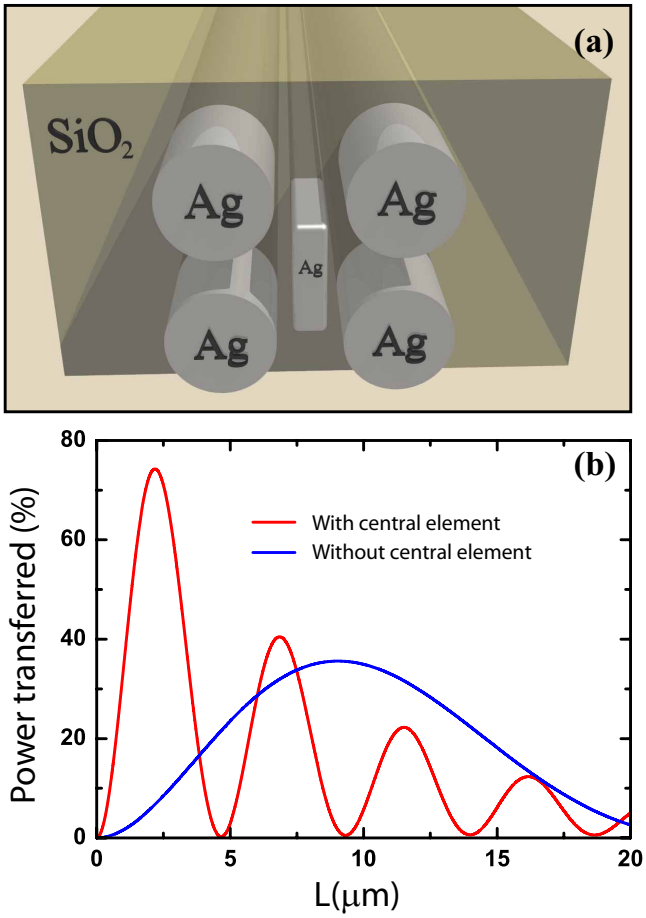

Fig. 5. Waveguide coupler consisting of an intermediate wire of rectangular cross section placed between the two gap-plasmon waveguides. (a) Schematic view of the geometry. (b) Fraction of power transferred between waveguides as a function of coupler length along the wires (solid curve). For comparison, we show the power transfer in two wire-pairs without intermediate coupler (dashed curve) for a distance $b = 20\,\text{nm}$. The transversal dimensions of the coupler are $140\,\text{nm} \times 20\,\text{nm}$. The four circular wires are arranged as in Fig. 1(b) with $d = 10\,\text{nm}$ and $b = 20\,\text{nm}$.

#116060 - $15.00 USD Received 24 Aug 2009; revised 23 Sep 2009; accepted 24 Sep 2009; published 12 Oct 2009

The Green function of these equations also captures the optical properties of the system. The Green function is implicitly defined by

$$\nabla\times\nabla\times\overleftrightarrow{G}(\mathbf{r},\mathbf{r}',\omega)-\frac{\omega^2}{c^2}\varepsilon(\mathbf{r})\overleftrightarrow{G}(\mathbf{r},\mathbf{r}',\omega)=\frac{-\overleftrightarrow{I}}{c^2}\delta(\mathbf{r}-\mathbf{r}'),\tag{4}$$

where $\overleftrightarrow{I}$ is the 3×3 unit tensor. This permits writing the electric field produced by any current distribution $\mathbf{j}(\mathbf{r},\omega)$ as

$$\mathbf{E}(\mathbf{r},\omega)=-4\pi\mathrm{i}\omega\int d\mathbf{r}'\overleftrightarrow{G}(\mathbf{r},\mathbf{r}',\omega)\cdot\mathbf{j}(\mathbf{r}',\omega).\tag{5}$$

The Green function can be expressed in terms of the eigenmodes as

$$\overleftrightarrow{G}(\mathbf{r},\mathbf{r}',\omega)=\sum_j\frac{\mathbf{E}_j(\mathbf{r})\otimes\mathbf{E}_j^*(\mathbf{r}')}{\omega^2-\omega_j^2+\mathrm{i}\gamma},\qquad\gamma\to0^+.\tag{6}$$

We can easily check that this is a solution of Eq. (4) by using Eq. (3), and by conveniently normalizing the wave functions, so that $\varepsilon(\mathbf{r})\sum_j\mathbf{E}_j(\mathbf{r})\otimes\mathbf{E}_j^*(\mathbf{r}')=\overleftrightarrow{I}\ \delta(\mathbf{r}-\mathbf{r}')$.

The photonic LDOS projected along some direction $\hat{\mathbf{n}}$, and defined as the combined projected local intensity of all eigenmodes for a given frequency ω, reads

$$LDOS(\mathbf{r},\omega)=\sum_j\left|\mathbf{E}_j(\mathbf{r})\cdot\hat{\mathbf{n}}\right|^2\ \delta(\omega-\omega_j).$$

This quantity can be also expressed in terms of the Green function as [15]

$$LDOS(\mathbf{r},\omega)=\frac{-2\omega}{\pi}\mathrm{Im}\left\{\hat{\mathbf{n}}\cdot\overleftrightarrow{G}(\mathbf{r},\mathbf{r},\omega)\cdot\hat{\mathbf{n}}\right\},$$

as deduced upon inspection of Eq. (6).

Noticing that a dipole of unit strength $\hat{\mathbf{n}}$ located at $\mathbf{r}_0$ is equivalent to a current density $-\mathrm{i}\omega\hat{\mathbf{n}}\delta(\mathbf{r}-\mathbf{r}_0)$, and inserting this into Eq. (5), the LDOS is obtained from the resulting field, evaluated at the position of the dipole:

$$LDOS(\mathbf{r}_0,\omega)=\frac{\omega^2\varepsilon^{1/2}}{3\pi^2c^3}+\frac{1}{2\pi^2\omega}\mathrm{Im}\left\{\hat{\mathbf{n}}\cdot\mathbf{E}^{\mathrm{ref}}(\mathbf{r}_0,\omega)\right\},\tag{7}$$

where we have separated the divergent direct dipole field to yield the LDOS in a homogeneous medium (first term in this equation), so that the remaining second term results from reflection of the dipole field at the boundaries of the structure under consideration. We use Eq. (7) in this paper to obtain the LDOS from the reflected field produced by a dipole.

For a frequency ω near a non-degenerate mode ω_j, the electric field can be approximated, according to Eqs. (5) and (6), as

$$\mathbf{E}(\mathbf{r},\omega)\approx A(\omega)\,\mathbf{E}_j(rb),$$

where

$$A(\omega)=\frac{-2\pi\mathrm{i}}{\varepsilon}\frac{1}{\omega-\omega_j+\mathrm{i}\gamma}\int d\mathbf{r}'\,\mathbf{E}_j(\mathbf{r}')\cdot\mathbf{j}(\mathbf{r}',\omega)$$

is a multiplicative constant. For degenerate modes, we can still recover the electric field for a single mode by choosing a current density $\mathbf{j}$ with the appropriate symmetry. We have used

#116060 - $15.00 USD Received 24 Aug 2009; revised 23 Sep 2009; accepted 24 Sep 2009; published 12 Oct 2009

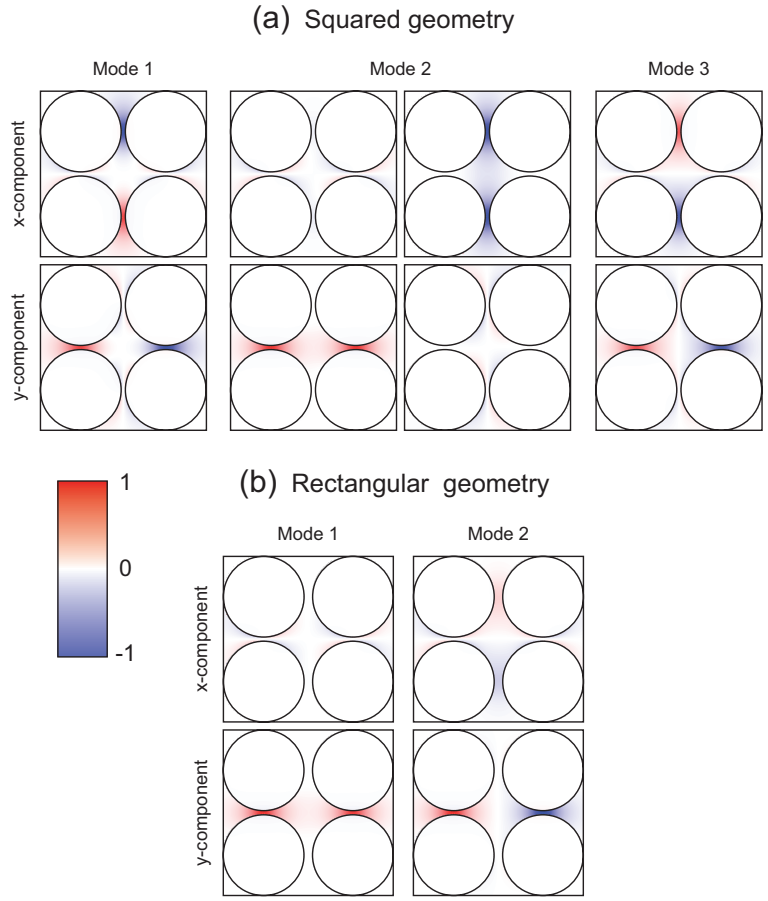

Fig. 6. Electric field for the modes of the symmetric 4-wire structure of Fig. 1(b) with $b = d = 10\,\text{nm}$. The light wavelength is $\lambda = 1000\,\text{nm}$ in all cases. Mode labels 1-3 are in correspondence with those of Fig. 2(b).

this properties to find the field distributions of some of the modes considered in this paper. For example, Figs. 6 and 7 show the electric field distributions for modes of a 4-fold symmetric structure and trimers, respectively. The arrows of the insets in Figs. 2 and 4 have been derived from Figs. 6 and 7. The above analysis must be slightly modified in the case of wires in order to decompose the field and the LDOS in terms of contributions arising from different q components [15]. In particular, the field distributions of Figs. 6 and 7 are constructed from the induced field for values of ω and q corresponding to the targeted mode, and with the external current $\mathbf{j}$ representing a dipole located at one of the gaps and oriented to be compatible with excitation of that mode.

Acknowledgments

This work has been supported in part by the Spanish MICINN (MAT2007-66050 and Consolider NanoLight.es) and by the EU (NMP4-2006-016881-SPANS and NMP4-SL-2008-213669-ENSEMBLE).

#116060 - $15.00 USD Received 24 Aug 2009; revised 23 Sep 2009; accepted 24 Sep 2009; published 12 Oct 2009

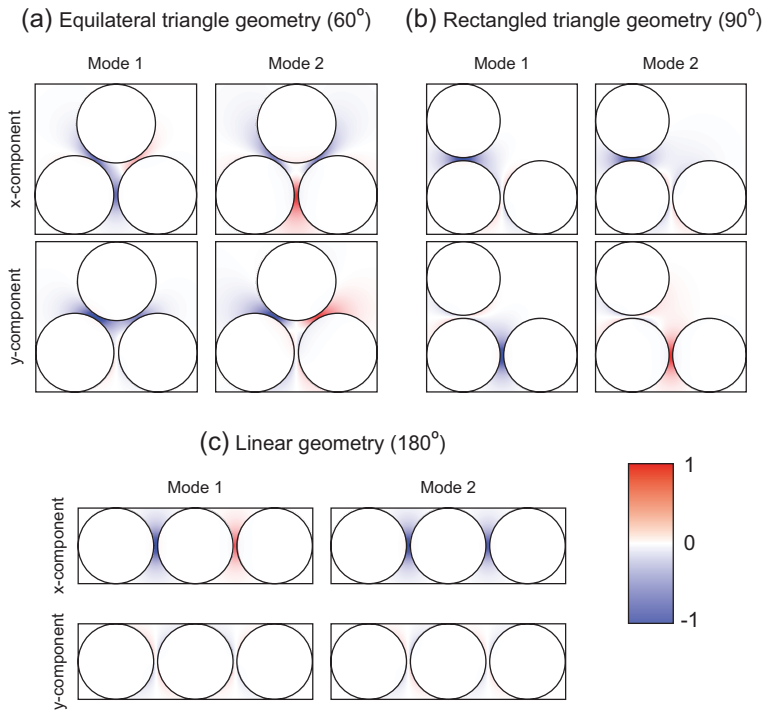

Fig. 7. Electric field for the modes of various trimer structures. The gap distance is $d = 10\,\text{nm}$ and the light wavelength is $\lambda = 1000\,\text{nm}$ in all cases.

#116060 - $15.00 USD Received 24 Aug 2009; revised 23 Sep 2009; accepted 24 Sep 2009; published 12 Oct 2009